2011

Ligand Fluorination to Optimize Preferential Oxidation of Carbon Monoxide by Water-Soluble Rhodium Porphyrins

Justin C. Biffinger
U.S. Naval Research Laboratory, Washington, DC, justin.biffinger@nrl.navy.mil

ShriHarsha Uppaluri
University of Nebraska-Lincoln

Haoran Sun
University of South Dakota

Stephen G. DiMagno
University of Nebraska-Lincoln, sdimagno@uic.edu

ACS Catalysis

RESEARCH ARTICLE

pubs.acs.org/acscatalysis

Ligand Fluorination to Optimize Preferential Oxidation of Carbon Monoxide by Water-Soluble Rhodium Porphyrins

Justin C. Biffinger,[†,‡] ShriHarsha Uppaluri,[†] Haoran Sun,[†,§] and Stephen G. DiMagno*[,†]

[†]Department of Chemistry and Nebraska Center for Materials and Nanoscience, University of Nebraska, Lincoln, Nebraska 68588-0304, United States

[‡]U.S. Naval Research Laboratory, Chemistry Division, Washington, D.C. 20375, United States

[§]University of South Dakota, Vermillion, South Dakota 57069, United States

Supporting Information

ABSTRACT: Catalytic, low temperature preferential oxidation (PROX) of carbon monoxide by aqueous [5,10,15,20-tetrakis-(4-sulfonatophenyl)-2,3,7,8,12,13,17,18-octafluoroporphyrinato]-rhodium(III) tetrasodium salt, (**1**[**Rh(III)**]) and [5,10,15,20-tetrakis(3-sulfonato-2,6-difluorophenyl)-2,3,7,8,12,13,17,18-octafluoroporphyrinato]rhodium(III) tetrasodium salt, (**2**[**Rh(III)**]) is reported. The PROX reaction occurs at ambient temperature in buffered ($4 \leq pH \leq 13$) aqueous solutions. Fluorination on the porphyrin periphery is shown to increase the CO PROX reaction rate, shift the metal centered redox potentials, and acidify ligated water molecules. Most importantly, β-fluorination increases the acidity of the rhodium hydride complex ($pK_a = 2.2 \pm 0.2$ for **2**[**Rh-D**]); the dramatically increased acidity of the Rh(III) hydride complex precludes proton reduction and hydrogen activation near neutral pH, thereby permitting oxidation of CO to be unaffected by the presence of H_2. This new fluorinated water-soluble rhodium porphyrin-based homogeneous catalyst system permits preferential oxidation of carbon monoxide in hydrogen gas streams at 308 K using dioxygen or a sacrificial electron acceptor (indigo carmine) as the terminal oxidant.

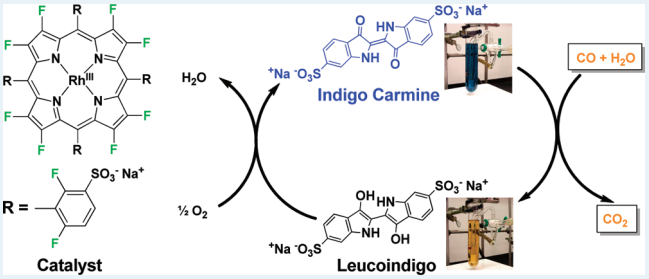

KEYWORDS: rhodium, fluorinated macrocycle, porphyrin, carbon monoxide, oxidation, fuel cells

INTRODUCTION

Pure hydrogen is the essential fuel for today's PEM (proton exchange membrane) fuel cells. While H_2 generated by electrolysis of water is generally pristine, hydrogen fuel streams produced by hydrocarbon,[1] alcohol,[2,3] or biomass[4−6] steam reforming are invariably contaminated with carbon monoxide (CO). Subsequent high temperature water gas shift (WGS) catalysis can reduce CO concentrations to the thermodynamic limit (20−50 ppm) in such H_2 gas streams.[2,7] However, the platinum anodes common in PEM fuel cells are poisoned by CO at concentrations as low as 10 ppm.[8] One solution to this problem is to develop catalytic methods to oxidize CO selectively, preferably below the PEM fuel cell operating temperature (353 K). Such a catalyst would enable CO removal without compromising the overall fuel cell efficiency. Design requirements for such catalysts are severe, since selective CO oxidation must be performed in the presence of H_2, CO_2, and water prior to entry of the gas into the fuel cell.[9]

Preferential oxidation (PROX) of CO can be performed either by capturing the reducing equivalents of CO at a fuel cell anode[10] (appropriate when the gas stream contains a high CO concentration), or by direct oxidation[11] of CO with air or O_2 if a relatively low concentration of CO is present (e.g., in H_2 streams produced by WGS catalysis). Previous work has shown that supported noble metal and metal oxide catalysts perform direct CO PROX; though these catalysts generally function efficiently only at or well above the PEM fuel cell operating temperature.[12−14] Noble metal clusters (Rh, Ru, Pt, Au) supported on alumina, zeolites, or mesoporous materials display good reactivity for CO PROX,[15−17] and excellent selectivity has been reported when Ru−Pt nanoparticles are used as the active catalysts.[18] PROX catalysts comprising less expensive metal oxides, such as CeO_2/CuO nanoparticle composites, show good specificity for CO (at 350 K) with comparable activity to alumina supported noble metals.[19−21] Though gold clusters and nanotubes have been explored for low temperature (0 °C) oxidation of CO, these catalysts have not proven to be as robust as mesoporous supported catalysts.[22]

Utilization of CO contaminant as a fuel for power generation has also been explored. Kubiak and co-workers constructed a PEM-CO/O_2 cell that utilized $[Rh(CO)_2Br]^-$ as a homogeneous CO oxidation catalyst, a graphite anode, and an oxygen reduction cathode.[23] Yamazaki and co-workers reported a

Special Issue: Victor S. Y. Lin Memorial Issue

Received: February 28, 2011
Revised: May 16, 2011
Published: May 18, 2011

CO-PEM/O_2 fuel cell system that featured immobilized rhodium octaethylporphyrins on carbon anodes; this cell was capable of generating 45 mW/cm^2 at 80 °C.[24] Dumesic and co-workers fabricated fuel cells featuring aqueous phosphomolybdic acid (a polyoxometallate, POM) and gold nanoparticle catalysts to oxidize CO and hydrogen simultaneously, thereby decreasing the gas purity requirements in their PEM fuel cell.[10,25] Phosphomolybdic acid (**PA**) functions as a multielectron redox mediator in this system, and it permits the use of untreated carbonaceous electrode materials to collect the reducing equivalents from the oxidation of hydrogen.

The study of discrete homogeneous transition metal complexes provides mechanistic insight useful for the design of selective CO oxidation catalysts. The porphyrin ligand offers a controlled environment for coordination of metal ions that bind carbon monoxide with the flexibility of tuning electron density on coordinated metal centers through peripheral substitution. Group IX transition metal metalloporphyrins are known to be good catalysts for diverse organic transformations such as alkane activation[26] and functionalization.[27] Cobalt and rhodium porphyrins in particular have been shown to catalyze carbon monoxide oxidation[28−32] and the insertion of CO into organometallic hydrides.[33] Rhodium and iridium porphyrins immobilized on Norit BRX support are active catalysts for CO oxidation.[31] It was posited that nucleophilic attack by water on the metal-coordinated CO molecule, an established reaction for Rh^{III} porphyrins first reported by Hendriksen and Eisenberg in 1976,[34] was the key step in this process. While construction of CO oxidation catalysts based upon rhodium porphyrins has ample precedent, application of these compounds for removal of CO from H_2 gas streams is compromised by their hydrogenase activity. We hypothesized that strong electron-withdrawing groups on the porphryin periphery could lead to more active CO oxidation catalysts while simultaneously reducing or eliminating hydrogen activation or proton reduction.

The rationale for our design of electron-deficient metalloporphyrin PROX catalysts is 3-fold: (1) removal of metal electron density by ligand substituents should increase the thermodynamic driving force and reduce the activation barrier for nucleophilic attack of water on CO, thereby enhancing activity, (2) the use of polar coordinating solvents should destabilize the Rh(II) state and enhance disproportionation,[35] thereby precluding direct hydrogen activation, and (3) the substituents should increase the acidity of rhodium hydrides (and increase the stability of Rh(I)) to such an extent that proton reduction will not occur. β-Fluorination of porphyrins is an effective approach to reduce the electron density of coordinated ligands without drastically changing the coordination sphere of the metal center.[36]

The impact of β-fluorination on porphyrin ring and chelated metal redox potentials has been studied extensively.[37] We have shown that fluorination of the porphyrin ring can shift the formal potential for the rhodium(II)/rhodium(I)$^-$ reversible redox couple by 540 mV in nonaqueous solutions[35] making these complexes excellent oxidants for a wide variety of reductants. Cyclic voltammetry experiments conducted in aqueous solutions showed that [5,10,15,20-tetrakis(4-sulfonatophenyl)-2,3,7,8,12,13,17,18-octafluoroporphyrinato]rhodium(III) exhibits significant redox potential shifts caused by β-fluorination, though the magnitudes of the shifts were slightly smaller than those measured for the nonionic derivatives in CH_2Cl_2.[38]

Here we report that heavily fluorinated water-soluble rhodium porphyrins are able to perform direct and indirect preferential CO oxidation catalysis under exceptionally mild conditions by the general mechanistic pathway outlined in Scheme 1. Fluorination of the porphyrin periphery is shown to enhance CO oxidation while simultaneously increasing selectivity. Fluorinated water-soluble rhodium porphyrins are able to selectively oxidize CO in H_2 streams at 308 K using sacrificial electron acceptors (e.g., indigo carmine) and oxygen as the terminal oxidant. Direct oxidation[11] of CO with air or O_2 is an attractive option for scrubbing trace CO from H_2 streams produced by WGS catalysis, since energy loss by direct oxidation is minimal under these conditions.

RESULTS AND DISCUSSION

Synthesis and Characterization of Rh(III) β-Fluorinated Water-Soluble Porphyrins. The syntheses of 2,3,7,8,12,13,17,18-octafluoro-5,10,15,20-tetraphenylporphyrin (F_8TPP)[38] and 2,3,7,8,12,13,17,18-octafluoro-5,10,15,20-tetrakis(2,6-difluorophenyl)porphyrin (F_{16}TPP)[39] and the sulfonation of F_8TPP and F_{16}TPP to form 5,10,15,20-tetrakis(4-sulfonatophenyl)-2,3,7,8,12,13,17,18-octafluoroporphyrin (**1**) and 5,10,15,20-tetrakis(2,6-difluoro-3-sulfonatophenyl)-2,3,7,8,12,13,17,18-octafluoroporphyrin (**2**), were performed as described previously.[39] The β-octafluorinatedporphyrin tetraanions were initially isolated as their tetraammonium salts, and subsequently metalated with $[Rh(CO)_2Cl]_2$ using a procedure adapted from the work of Krishnamurthy.[40] Ion-exchange to the sodium salt (DOWEX50WX8-100 resin, Na^+), filtration, and chromatography on a water-washed neutral aluminum oxide column afforded aquohydroxy[5,10,15,20-tetrakis(4-sulfonatophenyl)-2,3,7,8,12,13,17,18octafluoroporphyrinato]rhodium(III) tetrasodium salt, (**1**[**Rh(III)**]) and aquohydroxy[5,10,15,20-tetrakis(3-sulfonato-2,6-difluorophenyl)-2,3,7,8,12,13,17,18-octafluoroporphyrinato]rhodium(III) tetrasodium salt, (**2**[**Rh(III)**]) in 80−90% yields (Chart 1). Elemental analyses of these complexes showed that trace amounts of hydrated NaCl remained in the purified materials, even after chromatography in water.

Acid Dissociation Constants of Aquo Rh(III) β-Fluorinated Porphyrin Complexes. In aqueous solution binding of H_2 and CO by six-coordinate Rh(III) porphyrins is gated by deligation of axial water molecules. Thus, we investigated the general coordination properties of **1**[**Rh(III)**] and **2**[**Rh(III)**]. To mitigate complications arising from porphyrin-porphyrin interactions, porphyrin concentrations were kept <100 μM in titration experiments. Ashley et al.,[41] and more recently Wayland et al.,[42,43] reported that [5,10,15,20-tetrakis(4-sulfonatophenyl)porphyrinato]rhodium(III) (**3**[**Rh(III)**]) forms six-coordinate complexes in aqueous solution; the diaquo, aquohydroxo, or dihydroxo species predominates depending on the pH of the solution (Scheme 2).

Spectrochemical titration with aqueous sodium hydroxide [0.01−1 M] over the pH range 1−12 revealed three successive optical absorption spectra with clean isosbestic points. Analyses of the spectral changes in the Soret region sufficed to determine the relative concentrations of the diaquo, aquohydroxo, and dihydroxo at each pH. Equilibrium constants obtained from these analyses are listed in Table 1, along with literature data from comparable experiments conducted upon **3**[**Rh(III)**]. Linear least-squares fits for equilibria data are provided in the Supporting Information. These data show that porphyrin fluorination reduces the first acidity constant (pK_1) by more than one unit, but that pK_2 is surprisingly insensitive to fluorine substitution at

dx.doi.org/10.1021/cs2001187 |ACS Catal. 2011, 1, 764–771

the porphyrin β-positions. Such behavior is consistent with a leveling effect arising from significant additional donation of electron density from the axial aquo ligand once it is deprotonated. It is reasonable to expect that the bound hydroxide would contribute more electron-density into the more electron-deficient rhodium centers found in the fluorinated porphyrins.

Characterization of Rh(I) β-Fluorinated Water-Soluble Porphyrins. While Rh(III) porphyrins are typically axially ligated in aqueous solution, a two-electron reduction fills the metal d_{z^2} orbital, and is expected to result in deligation for Rh(I) porphyrin complexes. If relatively strongly coordinating ligands and/or anions are present in solution, an irreversible *apparently* 2-electron reduction (a typical ECE process, in which the first reduction is followed by rapid deligation and a second reduction[35,44]) is observed for rhodium(III) porphyrins. Complexes **1**[**Rh(III)**], **2**[**Rh(III)**], and **3**[**Rh(III)**] show an ECE reduction in alkaline aqueous solution (Table 1). The role coordinating ligands play in bringing about this disproportionation event has been thoroughly investigated.[35,44−46] Despite the relatively complex electrochemical behavior of these species, it is apparent from Table 1 that porphyrin fluorination shifts the Rh(III)/Rh(I) redox potential to more positive potentials under alkaline conditions. These experiments were performed at basic pH to ensure that only the dihydroxo species was present, thereby allowing a direct comparison of metal centers with identically charged coordination spheres. Because the axial ligands are contributing the greatest electron density to the rhodium center at this pH, the potentials reported should be an indication of the *minimum* impact of fluorination on the Rh(III) metal centers; at lower pH the impact of fluorination should be significantly larger.

Rh(I) porphyrins were prepared by electrochemical and chemical (alkaline sodium borohydride)[47] reduction, and these air-sensitive compounds were characterized by optical and NMR spectroscopies (Supporting Information). Reduction of **2**[**Rh(III)**] under alkaline conditions results in a shift of the Soret band from 403 to 383 nm. Hypsochromism upon reduction is diagnostic for formation of Rh(I) β-fluorinated porphyrins, such as cobaltacenium [2,3,7,8,12,13,17,18-octafluoro-5,10,15,20-tetrakis-(pentafluorophenyl)porphyrinato]rhodate in tetrahydrofuran.[27] The diamagnetic **2**[**Rh(I)**] complex generated a signal in the ^{19}F NMR spectrum (δ = −151 ppm) that was significantly upfield of that for the same signal in **2**[**Rh(III)**] (δ = −144 ppm). This relatively large shift of the β-fluorine signal stems from the sensitivity of the ^{19}F NMR resonance frequency to changes in metal ion electron density. Characteristically for nucleophilic Rh(I) porphyrins,[48−50] both **1**[**Rh(I)**]

Scheme 1. General Reaction Pathways for CO Oxidation Using Water-Soluble Rh(III) Porphyrins

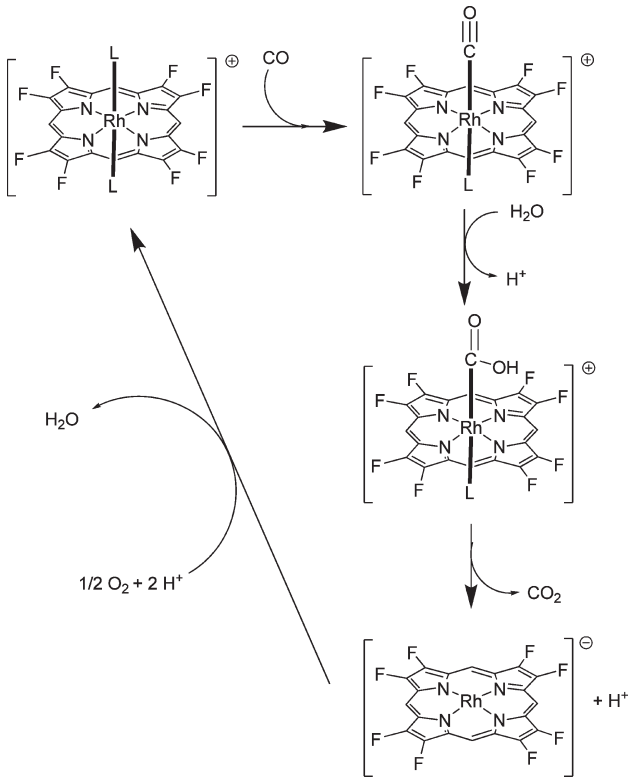

Chart 1. Water-Soluble Rhodium β-Fluorinated Porphyrins

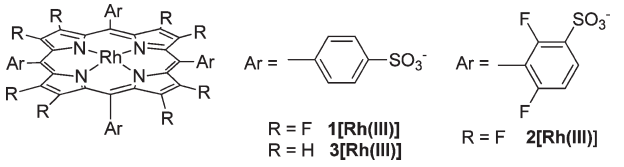

Table 1. Selected Physical Constants for Rh(III) Water-Soluble Porphyrins

compd.	pK_1	pK_2	E_{pc} [a]	E_{pa} [b]	ref.
1[**Rh(III)**]	5.9 ± 0.1	9.7 ± 0.2	−1.39	−0.30	[c]
2[**Rh(III)**]	5.7 ± 0.1	10.1 ± 0.1	−1.17	−0.20	[c]
3[**Rh(III)**]	7.01 ± 0.12	9.80 ± 0.24	−1.59[c]	−0.34[c]	42
compd.		p$K_{d(\text{Rh-D})}$			ref.
2[**Rh-D**]		2.2 ± 0.2			[c]
3[**Rh-D**]		7.1 ± 0.4			42

[a] Irreversible reduction in 0.5 M $NaPF_6$, 0.1 M NaOH, pH = 12.7, vs NHE. [b] E_{pa} irreversible oxidation reaction in 0.5 M $NaPF_6$, 0.1 M NaOH, pH 12.7 vs NHE. [c] This work.

Scheme 2. Acid Dissociation Equilibria for Bis Aquo Rh(III) Water-Soluble Porphyrins[a]

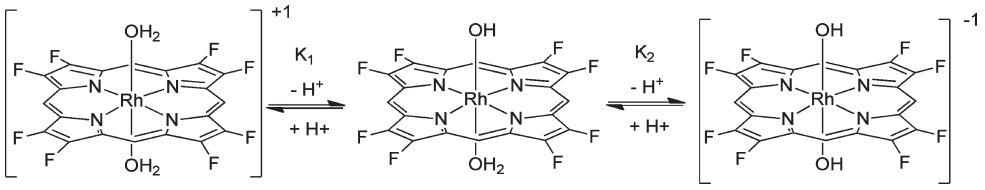

[a] The meso-aryl groups were omitted for clarity.

dx.doi.org/10.1021/cs2001187 |ACS Catal. 2011, 1, 764–771

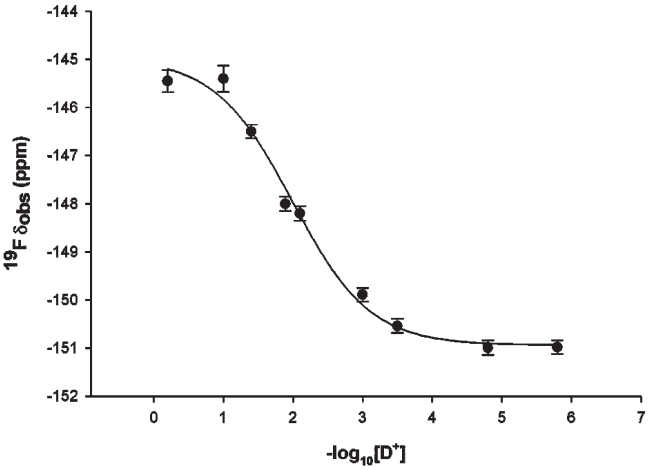

Figure 1. Determination of acid dissociation constant pK_a for **2**[**Rh-D**] by ^{19}F NMR spectroscopic titration.

and **2**[**Rh(I)**] were alkylated with methyl iodide under standard conditions.[42] The methylated complexes were identified by the chemical shift of the shielded Rh-CH_3 methyl group signal (δ = −6.61 and −6.31 ppm for **1**[**Rh-CH_3**] and **2**[**Rh-CH_3**], respectively) in the ^{1}H NMR spectrum. Solutions of **1**[**Rh(I)**] and **2**[**Rh(I)**] are oxidized rapidly (<10 s) to regenerate **1**[**Rh(III)**] and **2**[**Rh(III)**] quantitatively upon exposure to air or purified dioxygen.

Acid Dissociation Constants for Rh(III) Deuteride Porphyrin Complexes. The M-D acidity of deuterido[5,10,15,20-tetrakis(4-sulfonatophenyl)porphyrinato]rhodate (**3**[**Rh-D**]) was reported by Wayland and co-workers;[42] the pK_a of this species was calculated to be 7.1 ± 0.4 (Table 1). Since fluorination of the porphyrin periphery has a substantial effect on the Rh(I)/Rh(III) redox potential and acidifies pendant aquo ligands, it was expected that the pK_a of the metal deuteride **2**[**Rh-D**] would be significantly lower than 7.1. The pK_a of **2**[**Rh-D**] was determined by titrating degassed D_2O solutions containing **2**[**Rh(I)**] under H_2 (1 atm), and monitoring the ^{19}F NMR chemical shift of the β-fluorine signals as a function of solution pH. (The hydrogen blanket was necessary to suppress the oxidation of **2**[**Rh(I)**] by a proton reduction pathway). Because independent measurements established the chemical shifts for the β-fluorine resonances in **2**[**Rh-D**] (δ = −146 ppm) and **2**[**Rh(I)**] (δ = −151 ppm), the pH at the midpoint of this chemical shift range (Figure 1) pegged the pK_a for **2**[**Rh-D**]. Control experiments confirmed that the β-fluorine signal was only sensitive to solution pH; a change in buffer composition or overall ionic strengths did not affect this chemical shift reporter. The pK_a for **2**[**Rh-D**] is 2.2 ± 0.2.

The increased acidity of **2**[**Rh−H**] assures that only the clean, two electron reduction of **2**[**Rh(III)**] will be observed under mildly acidic to alkaline conditions upon exposure to CO. Unfortunately, **1**[**Rh(I)**] is sufficiently basic to form the metal hydride **1**[**Rh−H**], which collapses to a dimeric, unreactive Rh(II) species under neutral to acidic conditions. The mechanism for **1**[**Rh(II)**] formation was unexplored, but presumably this occurs by proton reduction; discrete monomeric Rh(II) intermediates were not observed.[45] Dimerization of Rh(II) porphyrins is well documented for complexes not containing bulky ortho-substituents on the meso-aryl rings.[33] Apparently, the Rh−Rh bond is sufficiently strong to frustrate disproportionation for **1**[**Rh(II)**], and this complex is trapped in this low energy dimer. In contrast, under alkaline conditions, chemical and electrochemical reduction of **1**[**Rh(III)**] yielded **1**[**Rh(I)**] as the only species observed by ^{19}F NMR spectroscopy (Supporting Information). The anaerobic oxidation of **1**[**Rh(I)**] and subsequent dimerization of **1**[**Rh(II)**] contrasts with the behavior of **2**[**Rh(I)**], which is monomeric under acidic and basic conditions. While electronic tuning of the metal center and coordinating solvent preclude easy formation of stable Rh(II) intermediates for this compound, it has also been shown previously that four meso-2,6-difluoroaryl substituents provide sufficient steric bulk to thwart dimer formation in the event that any Rh(II) porphyrin would form.[33]

We have demonstrated previously that β-fluorination has a significant impact upon porphyrin ring and chelated metal ion electronic properties.[27,38,51,52] In keeping with these observations, the rhodium center of the water-soluble derivative **2**[**Rh-(III)**] has a more positive reduction potential (−1.17 V, pH = 12.7, 0.5 M $NaPF_6$) in aqueous solution than that of **1**[**Rh(III)**] (−1.59 V) under identical conditions (Table 1). Similarly, the pK_d of the Rh(III) deuteride **2**[**Rh-D**] (pK_d = 2.2 ± 0.2) is considerably lower than that measured by Wayland for **3**[**Rh-D**] (pK_d = 7.1 ± 0.4) (Table 1). The dramatic increase in the hydride acidity caused by fluorination precludes hydrogen activation near neutral pH, potentially permitting PROX of CO in the presence of H_2.

Reactivity of Rh(III) β-Fluorinated Porphyrins with Carbon Monoxide. In phosphate buffer **1**[**Rh(III)**] (like **2**[**Rh(III)**]) exists as the diaquo complex at pH = 4, and as the dihydroxy complex at pH = 13; thus CO oxidation was examined initially at these two pH levels to simplify the coordination chemistry. When basic (100 mM NaOH) degassed D_2O solutions of **1**[**Rh(III)**] and **2**[**Rh(III)**] were sealed under CO (1 atm) at room temperature, characteristic upfield shifts (β-fluorine δ = −144 ppm → δ = −151 ppm, Figure 2) in the ^{19}F NMR spectra were noted; these observations are consistent with the formation Rh(I) porphyrins. The observed rate constant for the reduction of **2**[**Rh(III)**] (k = 14 ± 1.3 M^{-1} s^{-1}) was almost 100 times that of **1**[**Rh(III)**] (k = 0.2 ± 0.02 M^{-1} s^{-1}). **1**[**Rh(III)**] was not regenerated upon exposure of the solution of **1**[**Rh(I)**] to air. Instead, a stable Rh-peroxo complex was observed (Supporting Information). In contrast, **2**[**Rh(III)**] was regenerated immediately upon venting the NMR tube containing an aqueous solution of **2**[**Rh(I)**], suggesting that the fluorinated complex might be able to use dioxygen as the terminal oxidant for CO oxidation.

After survey of reaction conditions to optimize catalyst stability and reaction rate, 35 °C pH = 4 sodium phosphate buffer (200 mM) was adopted as the standard set of conditions for the remaining experiments. Two different techniques were used to measure CO oxidation kinetics under multiple turnover conditions. In the first method a sacrificial oxidant, indigo carmine (IC), was used as an indicator dye (Scheme 3); the oxidized, dark blue form of the dye is reduced rapidly by **2**[**Rh(I)**] to generate the colorless leuco derivative. Thus, the bleaching of a measured amount of dye served as a convenient (and sharp) titration end point indicating generation of a known quantity of **2**[**Rh(I)**] (Figure 3). In a typical experiment an aqueous solution of **2**[**Rh(III)**] (0.025 mM−0.25 mM) containing a measured amount of IC (1−100 equiv.) was degassed under dynamic vacuum. The vigorously agitated solution was placed under CO (1 atm), and the time to the end point (dye bleaching)

dx.doi.org/10.1021/cs2001187 |ACS Catal. 2011, 1, 764–771

was measured. The turnover frequency (TOF) remained constant (1.8−2.0 TO min^{-1}) over this porphyrin concentration range. When the CO concentration was diluted to 0.5 atm with either 50% N_2 or 50% H_2 carrier, the TOF was also halved. The measured TOF corresponds to a bimolecular rate constant of $35 \pm 3\ M^{-1}\ s^{-1}$ for CO oxidation at 35 °C. It is notable that the TOF for CO oxidation was unaltered by the presence of hydrogen; TOF values depended only on the partial pressure of CO. There was also no observable formation of **2[Rh(I)]** from **2[Rh(III)]** with pure H_2 (1 atm) under the conditions of the CO oxidation experiments (as determined by examination of the UV−vis and ^{19}F-NMR spectroscopy).

Several sources of error in the rate constant measurements were probed by varying the concentration of **2[Rh(III)]** in titration experiments. At low **2[Rh(III)]** concentration and in experiments run at low turnover numbers, an induction period was required to scrub the residual oxygen contaminant remaining after sample preparation. At high porphyrin concentration (>0.5 mM) mass transfer of the sparingly soluble (8.7×10^{-4} M at 1 atm)[53] CO resulted in reduced measured TOFs. Nevertheless, consistent and reproducible turnover numbers were achieved at intermediate catalyst concentrations (0.025 mM−0.25 mM) at 1 atm CO pressure (Supporting Information).

The redox mediator indigo carmine (IC) plays two important roles in the rhodium porphyrin-catalyzed CO oxidation. First, it is a very efficient oxidant for **2[Rh(I)]**; UV−vis spectra gathered under turnover conditions showed that **2[Rh(III)]** was the only porphyrin species present as long as oxidized IC remained in solution, indicating that dye-mediated oxidation of **2[Rh(I)]** is extremely fast and that reoxidation of the catalyst was not rate limiting (Supporting Information). A second, equally important role for the leuco form of IC is as a redox buffer that is capable of scavenging strong oxidants in the presence of **2[Rh(III)]**. In the absence of indigo carmine, rapid catalyst decomposition was observed. For example, if a buffered D_2O solution of **2[Rh(III)]** was cycled repeatedly through a three step (degassing/CO/air) sequence, the formation of free fluoride (detected by ^{19}F-NMR spectroscopy) and bleaching of the **2[Rh(III)]** optical signature were apparent after fewer than 10 turnovers. In contrast, when IC was present in 10-fold excess compared to **2[Rh(III)]**, 10 degassing/CO/air cycles could be performed to oxidize more than 100 equiv of CO without measurable loss in catalytic activity. Given that **2[Rh(III)]** is unstable in the presence of hydrogen peroxide, we suspected that H_2O_2 generated by dioxygen reduction was responsible for porphyrin decomposition. Rotating ring-disk voltammetry confirmed that **2[Rh(I)]** reduces dioxygen by two- and four-electron processes at approximately equal rates at pH = 4, so H_2O_2 was confirmed as a significant byproduct of CO oxidation when dioxygen was the terminal oxidant (Supporting Information). Finally, we confirmed that the reduced dye is rapidly oxidized by H_2O_2 in the presence of **2[Rh(III)]**. These observations indicate that IC is acting as a catalyst preservative by scavenging active oxygen species. As long as the reduced form of the dye is present, air can be used as the terminal oxidant for **2[Rh(III)]** catalyzed PROX of carbon monoxide.

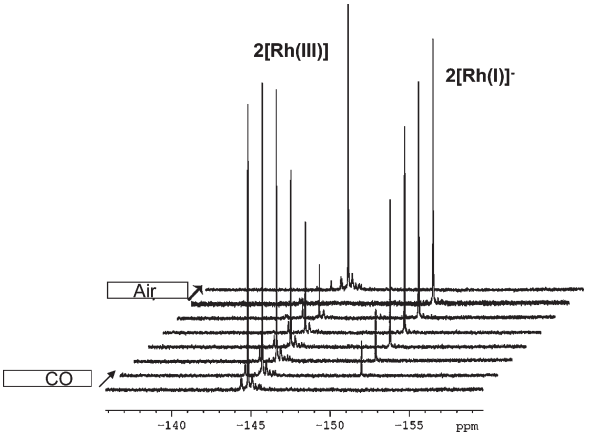

Figure 2. Changes in the ^{19}F NMR during the reaction of **2[Rh(III)]** with CO in D_2O. The peaks at 145 ppm and −151 ppm arise from the β−F on **2[Rh(III)]** and **2[Rh(I)]**$^-$ respectively.

Evaluation of 2[Rh(III)] as a PROX Catalyst for CO in Hydrogen. To show the general applicability of these compounds as PROX catalysts within fuel cells, the most active catalyst (**2[(Rh(III)]**) was placed under an atmosphere of hydrogen or carbon monoxide in a sealed cuvette in 100 mM sodium hydroxide solution and the reduction of **2[Rh(III)]** to **2[Rh(I)]** was followed by UV−vis spectroscopy at 50 and 30 °C, respectively (Figure 4). Under these conditions, only the reaction of **2[(Rh(III)]** with carbon monoxide was observed. The oxidation of CO catalyzed by **2[Rh(III)]** was also monitored by head gas analysis in a mixture of CO balanced with H_2 or N_2. In a typical experiment a degassed buffered aqueous solution of **2[Rh(III)]** (0.6 mM) and IC (6.0 mM) was charged with 1 atm of a gas mixture containing CO and H_2. Head gas analysis by gas chromatography (Figure 5) confirmed that CO was consumed, that CO_2 was generated during the course of the reaction, and that H_2 was not oxidized simultaneously, even when residual dioxygen was present. Head gas analysis demonstrated conclusively that CO can be scrubbed from hydrogen gas streams by **2[Rh(III)]** to generate CO_2.

In summary, we have demonstrated that the introduction of fluorine substituents into water-soluble rhodium porphyrins lowers the pK_a of the metal hydride, thereby permitting these complexes to act as effective low-temperature, low pressure homogeneous PROX catalysts for CO. The indicator dye indigo carmine serves as a redox reservoir providing reducing equivalents that effectively scavenge active oxygen species. The combination of **2[Rh(III)]** and IC under both alkaline and neutral conditions comprise a robust catalyst system capable of selectively oxidizing CO in H_2 streams using air as the terminal

Scheme 3. Redox Equilibrium of Indigo Carmine and Leucoindigo

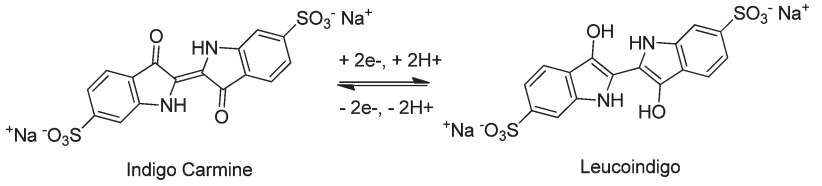

Indigo Carmine Leucoindigo

dx.doi.org/10.1021/cs2001187 |ACS Catal. 2011, 1, 764–771

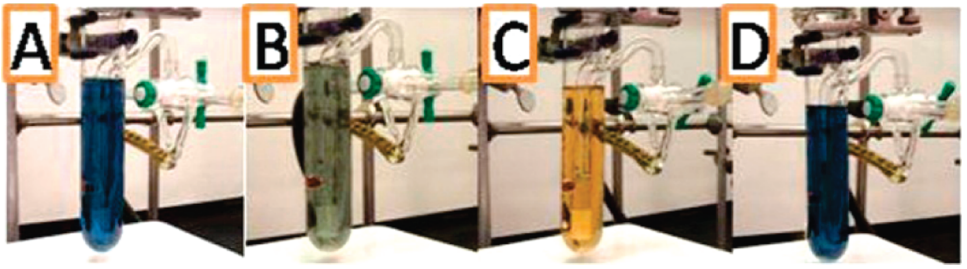

Figure 3. Reaction of **2[Rh(III)]** with CO in the presence of 100 equiv of indigo carmine: (a) initial, (b) after CO introduction, (c) at reaction end point, ans (d) after exposure to air.

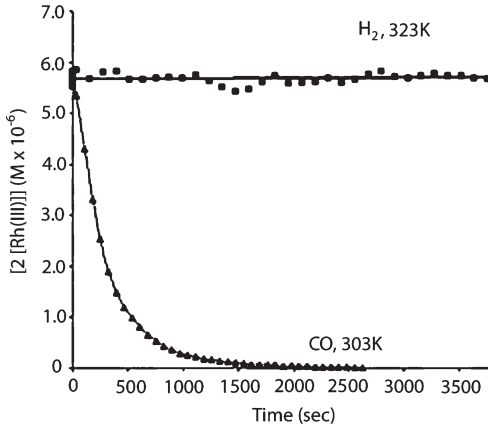

Figure 4. Comparison of the reaction of **2[Rh(III)]** with carbon monoxide or hydrogen.

oxidant. Although the maximum turnover frequency obtained with the rhodium porphyrin catalytic system is modest, the strategy of using ligand substituent effects to tune metal hydride acidity, control proton reduction, and preclude hydrogen activation provides a rational framework for optimizing more robust and active Rh-based PROX catalysts.

EXPERIMENTAL SECTION

Reagents and General Techniques. 2,3,7,8,12,13,17,18-Octafluoro-5,10,15,20-tetraphenylporphyrin[38] and 2,3,7,8,12,13,17,18-octafluoro-5,10,15,20-tetrakis(2,6-difluorophenyl)porphyrin[39] were prepared according to literature methods. Reagents were supplied from Aldrich, Sigma, Fisher, Fluka, or Cambridge Isotope Laboratories and used as received unless otherwise indicated. NMR spectra were obtained in D_2O or d_4-MeOH using the 400, 500, and 600 MHz spectrophotometers at the University of Nebraska-Lincoln. ^{19}F NMR spectra were collected at 470 or 376 MHz in the same solvents using hexafluorobenzene as a chemical shift reference (δ = −164.9 ppm). Research grade gases and gas mixes were purchased from Linweld, Lincoln, NE. Absorption spectra were obtained using modified (OLIS-14) Cary-14 UV−vis−NIR or Varian Cary 5000 spectrophotometers equipped with a variable-temperature cell holder and a circulating bath (Laude RC3). Analyses of gaseous reaction components were performed on a Varian CP-3800 equipped with HayeSep Q 80/100 mesh and Supelco 13X molecular sieve 45/60mesh columns with valved systems, and a thermal conductivity detector (TCD). A Fisher Scientific Accumet meter with a combination pH electrode (Ag/AgCl reference, gel-filled) was used for pH determinations. Mass spectra were collected at the University of Nebraska Center for Mass Spectrometry. Elemental analyses were conducted by QTI, Whitehouse, NJ.

Synthesis of Rhodium(III) 5,10,15,20-Tetrakis(4-sulfonatophenyl) 2,3,7,8,12,13,17,18-octafluoroporphyrin Diaquo Tetrasodium Salt, 1[Rh(III)]. 2,3,7,8,12,13,17,18-Octafluoro-5,10,15,20-tetrakis(4-sulfonatophenyl)porphyrin[39] tetraammonium salt (65 mg, 0.057 mmol) was dissolved in methanol. $[Rh(CO)_2Cl]_2$ (22 mg, 0.057 mmol) was added directly to the porphyrin solution. The mixture was heated (50−60 °C) for 15 h, and the reaction progress was monitored periodically by UV−visible spectroscopy. The solvent was evaporated, and the crude material was dissolved in deionized water, loaded onto a column containing DOWEX 50WX8 ion-exchange resin (Na^+ salt), and eluted with H_2O until the column discharge was colorless. The collected fractions were loaded directly onto a water-washed neutral aluminum oxide column, and the porphyrin was eluted with a 0.02 M NaOH solution. After the solvent was evaporated to dryness, and the residue was dissolved in 10 mL of methanol. This methanol solution was filtered through a 0.20 μm HPLC syringe filter (Fisherbrand, PTFE) prior to precipitation with diethyl ether. The solid was collected by filtration (Osmonics/MSI Magna Nylon Membrane filter (0.45 μm)) and dried in vacuo. The yield of **1[Rh(III)]** was 69 mg (94%). The NMR spectra of the fluorinated porphyrins indicate that several differently ligated species are present in buffered water; only the major species is described: ^{19}F NMR (470 MHz, D_2O, 20 mM phosphate buffer, pH 7): δ = −141.24 (s, 8F); ^1H NMR (500 MHz, D_2O, 20 mM phosphate buffer, pH 7): δ = 8.15 (d, 8H, J = 10 Hz), 8.03 (d, 8H, J = 10 Hz); UV-vis (20 mM phosphate buffer, pH 7): λ_{max} (ε) = 398 (150000), 515 (18000), 549 nm (6000); MS (low res FAB pos. ion): m/z 1285 [$C_{44}H_{18}F_8N_4Na_4O_{13}RhS_4$ 1285.74]; elemental analysis calcd-(%) for $C_{44}H_{26}F_8N_4Na_6O_{21}RhS_5$ (1498.80): C 35.23, H 1.75, N 3.74; found: C 35.48, H 1.52, N 3.64.

Synthesis of Rhodium(III) 5,10,15,20-Tetrakis(3-sulfonato-2,6-difluorophenyl) 2,3,7,8,12,13,17,18-octafluoroporphyrin Diaquo Tetrasodium Salt, 2[Rh(III)]. A similar procedure was used as for **1[Rh(III)]**. The yield of **2[Rh(III)]** was (92%): ^{19}F NMR (470 MHz, D_2O, 20 mM phosphate buffer, pH 7): δ = −107.05 (m, 4F), −110.76 (m, 4F), −144.92 (s, 8F); ^1H NMR (500 MHz, D_2O, 20 mM phosphate buffer, pH 7): δ = 8.35 (m, 4H), 7.63 (m, 4H); UV-vis (20 mM phosphate buffer, pH 7): λ_{max} (ε): 399 (140000), 518 (14000), 550 nm (4300); MS (high res FAB pos. ion): m/z 1412.7674 ($C_{44}H_8F_{16}N_4Na_4O_{12}RhS_4$ 1412.7568); elemental analysis calcd (%) for $C_{44}H_{18}ClF_{16}N_4Na_4O_{17}RhS_4$ (1535.76): C 34.38, H 1.18, N 3.64; found: C 34.16, H 0.82, N 3.45.

dx.doi.org/10.1021/cs2001187 |ACS Catal. 2011, 1, 764–771

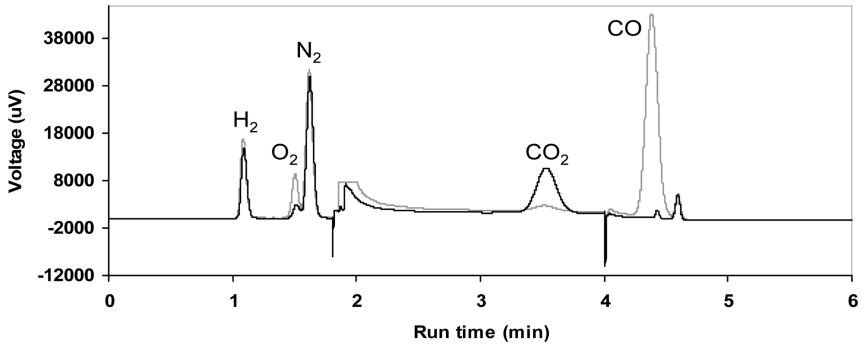

Figure 5. Reaction of CO from a mixture of 10% CO in H_2 (total pressure of 1 atm) by a pH 4 solution of 0.6 mM **2**[**Rh(III)**] and 6.0 mM indigo carmine at 35 °C. Initial head gas sample, gray line; final head gas sample, black line. N_2 and O_2 were introduced when the head gas was injected into the GC.

Synthesis of Meso-tetrakis(*p*-sulfonatophenyl)porphyrinato-rhodate(III), [RhTSTPP, 3[Rh(III)]]. 5,10,15,20-Tetrakis(4-sulfonatophenyl)porphyrin (sodium salt) was purchased from Aldrich and used as received. The rhodium insertion was modified from previous work[41] to the insertion conditions used for **1**[**Rh(III)**] and **2**[**Rh(III)**]. The analytical data were identical to published work.[7,41]

In Situ Generation of [2,3,7,8,12,13,17,18-Octafluoro-5,10,15,20-tetrakis(3-sulfonato-2,6-difluorophenyl)porphyrinato]rhodium(I) Tetrasodium Salt, 2[Rh(I)]. A 1 mM solution of **2**[**Rh(III)**] (0.5 mL in D_2O was degassed with a stream of nitrogen in a NMR tube sealed with a septum. A 0.1 mL aliquot of a 20 mM solution of sodium borohydride in degassed 0.5 M sodium hydroxide (diluted with deuterium oxide) was added via syringe. The color changed from dark brown to light orange immediately. Upon reduction, only one species is evident in the NMR spectrum due to ligand loss: ^{19}F NMR (376 MHz, D_2O/NaOH, pH 10): δ = −107.10 (m, 4F), −109.76 (m, 4F), −151.09 (s, 8F); ^{1}H NMR (400 MHz, D_2O/NaOH, pH 10): δ = 8.07 (q, 8H, J = 8 Hz), 7.53 (t, 4H, J = 8 Hz); UV-vis (20 mM phosphate buffer, pH 7): λ_{max} (ε) = 383 (140000), 484 (2700), 508 nm (3700).

In Situ Generation of [2,3,7,8,12,13,17,18-Octafluoro-5,10,15,20-tetrakis(4-sulfonatophenyl)porphyrinato]diaquo Rhodium Tetrasodium Salt, 1[Rh(I)]. The procedure used to generate **2**[**Rh(I)**] was also used for this complex. ^{19}F NMR (376 MHz, D_2O/NaOH, pH 10): δ = −148.04 (s, 8F); ^{1}H NMR (400 MHz, D_2O/NaOH, pH 10): δ = 7.95 (m, 8H), 7.67 (m, 8H); UV-vis (D_2O/NaOH, pH 9): λ_{max} (ε) = 390 (110000), 488 (13000), 480 nm (7800).

Synthesis of Methyl [2,3,7,8,12,13,17,18-Octafluoro-5,10,15,20-tetrakis(4-sulfonatophenyl)porphyrinato]rhodium Tetrasodium Salt, 1[Rh-CH$_3$]. Excess CH_3I (1.0 mL) was added to an ethanol solution (20 mL) of **1**[**Rh(I)**] (25 mg, 0.019 mmol) under a nitrogen atmosphere. The reaction was stirred under nitrogen in the absence of light for 12 h. The solution was dried over sodium sulfate prior to precipitation of **1**[**Rh-CH$_3$**] with diethyl ether. After the third precipitation, this complex was sufficiently pure for analysis. Yield: 20 mg (82%). ^{19}F NMR (376 MHz, D_2O, pH 8): δ = −142.64 (s, 8F); ^{1}H NMR (400 MHz, D_2O, pH 8): δ = 8.15 (broad d, 8H, J = 8 Hz), 8.05 (m, 8H), −6.61 (broad s, 3H); ^{19}F NMR (470 MHz, DMSO-d_6): δ = −144.16 (s, 8F); ^{1}H NMR (500 MHz, DMSO-d_6): δ = 8.02−7.87 (m, 16H), −6.33 (broad s, 3H).

UV-vis (20 mM phosphate buffer, pH 7): λ_{max} (ε) = 403 (150000), 520 nm (12000).

Synthesis of Methyl [2,3,7,8,12,13,17,18-Octafluoro-5,10,15,20-tetrakis(3-sulfonato-2,6-difluorophenyl)porphyrinato]rhodium Tetrasodium Salt, 2[Rh-CH$_3$]. A procedure similar to that used to prepare **1**[**Rh-CH$_3$**] was employed. ^{19}F NMR (376 MHz, 20 mM phosphate buffer, pH 7): δ = −105.05 (m, 4F), −109.34 (m, 4F), −146.24 (s, 8F); ^{1}H NMR (400 MHz, 20 mM phosphate buffer, pH 7): δ = 8.21 (m, 4H), 7.49 (m, 4H), −6.31 (d, 3H, J = 18 Hz); UV-vis (20 mM phosphate buffer, pH 7): λ_{max} (ε) = 399 (180000), 516 (13000), 544 nm (4500).

Kinetic Measurements for the Determination of TOF$_{av}$ of the 2[Rh(III)] Catalyzed Oxidation of CO by Indigo Carmine. A J. Young tube was charged with 1 mL of an aqueous solution (buffered at pH 4 with a 200 mM phosphate buffer) of **2**[**Rh(III)**] and IC at the required concentration. The blue colored solution was degassed by cool (0 °C)-pump-warming (35 °C) ten times directly on a Schlenk line. The tube was then pressurized (1 atm) with pure CO or 50% CO in (N_2 or H_2) through a mercury bubbler. The solution was agitated for 30 s by flip-flopping and tapping the tube to ensure quick introduction of a uniform concentration of CO into solution. The tube was then placed in a 35 °C water bath. The tube was removed from the heating bath every 1.5 min, and the solution agitated as described above for 15 s, and was then returned to the heating bath. This procedure was repeated until the blue color of the solution disappeared leaving behind a brown colored solution, which is the color of **2**[**Rh(III)**]. Kinetics data are included in the Supporting Information.

Scrubbing CO from H_2. A Schlenk flask (total volume 12 mL) was charged with 8.5 mL of an aqueous solution (buffered at pH 4 with a 200 mM phosphate buffer) of **2**[**Rh(III)**] (0.6 mM) and IC (6.0 mM). A magnetic stir bar was dropped in, and the flask was sealed with a rubber septum. The solution was degassed by freeze−pump−thawing three times on the Schlenk line. The flask was then pressurized (1 atm) with the required gas mix (10% CO in H_2 or 1% CO in H_2) through a mercury bubbler. The flask was then transferred to an oil bath maintained at 35 °C, and the solution was set to vigorous stirring. Twenty-five microliter aliquots of the head gas were withdrawn using a gastight syringe, initially, and from time to time through the progress of the reaction, and analyzed by GC.

Determination of the pK_a of D-RhTSF$_{16}$TPP (2[Rh-D]). Samples of **2**[**Rh(III)**] loaded into J. Young NMR tubes (in

dx.doi.org/10.1021/cs2001187 |*ACS Catal.* 2011, 1, 764–771

deuterium oxide, 20 mM phosphate, acetate, or oxalate buffers) were degassed via Schlenk techniques. The evacuated tubes were pressurized with H_2 (1.0 atm), and ^{19}F NMR were collected to determine the acid dissociation constant (298 K, C_6F_6 int. std.). The observed ^{19}F chemical shift of the β-signal was independent of buffer composition, but strongly dependent on pH. The pH was monitored with a properly calibrated combination pH electrode before and after the NMR experiment. The data were linearized using the Henderson−Hasselbalch equation using the observed NMR shifts and fit with the standard linear regression package in Mathematica 5.0. The limiting chemical shift values used were $\mathbf{2}[\mathbf{Rh\text{-}D}] = -146$ ppm and $\mathbf{2}[\mathbf{Rh(I)}] = -151$ ppm.

■ ASSOCIATED CONTENT

Supporting Information. NMR, UV−vis and GC spectra, details of kinetic studies and experimental procedures. This material is available free of charge via the Internet at http://pubs.acs.org.

■ AUTHOR INFORMATION

Corresponding Author

*Phone: 1-402-472-9895. Fax: 1-402-472-9402. E-mail: sdimagno1@unl.edu.

Funding Sources

The work was supported through the ONR and DARPA (N66001-08-1-2026) for support of the research and the National Institutes of Health (RR016544-01) for laboratory infrastructure.

■ REFERENCES

(1) Ming, Q.; Healey, T.; Allen, L.; Irving, P. *Catal. Today* **2002**, *77*, 51.
(2) Davda, R. R.; Dumesic, J. A. *Angew. Chem., Int. Ed.* **2003**, *42*, 4068.
(3) Joensen, F.; Rostrup-Nielsen, J. R. *J. Power Sources* **2002**, *105*, 195.
(4) Cortright, R. D.; Davda, R. R.; Dumesic, J. A. *Nature (London)* **2002**, *418*, 964.
(5) Jacobsen, H. *Angew. Chem., Int. Ed.* **2004**, *43*, 1912.
(6) Marquevich, M.; Czernik, S.; Chornet, E.; Montane, D. *Energy Fuels* **1999**, *13*, 1160.
(7) Fu, Q.; Saltsburg, H.; Flytzani-Stephanopoulos, M. *Science (Washington, DC)* **2003**, *301*, 935.
(8) Stonehart, P.; Kohlmayr, G. *Electrochim. Acta* **1972**, *17*, 369.
(9) Kolb, G. *Fuel Processing for Fuel Cells*; Wiley-VCH Verlag: Weinheim, Germany, 2008.
(10) Kim, W. B.; Voitl, T.; Rodriguez-Rivera, G. J.; Evans, S. T.; Dumesic, J. A. *Angew. Chem., Int. Ed.* **2005**, *44*, 778.
(11) Fukuoka, A.; Kimura, J.-I.; Oshio, T.; Sakamoto, Y.; Ichikawa, M. *J. Am. Chem. Soc.* **2007**, *129*, 10120.
(12) Xu, L.; Ma, Y.; Zhang, Y.; Jiang, Z.; Huang, W. *J. Am. Chem. Soc.* **2009**, *131*, 16366.
(13) Rico, V. J.; Hueso, J. L.; Cotrino, J.; Gallardo, V.; Sarmiento, B.; Brey, J. J.; Gonzalez-Elipe, A. R. *Chem. Commun.* **2009**, 6192.
(14) Deng, W.; Flytzani-Stephanopoulos, M. *Angew. Chem., Int. Ed.* **2006**, *45*, 2285.
(15) Faur Ghenciu, A. *Curr. Opin. Solid State Mater. Sci.* **2002**, *6*, 389.
(16) Kim, Y. H.; Park, E. D.; Lee, H. C.; Lee, D.; Lee, K. H. *Catal. Today* **2009**, *146*, 253.
(17) Ishida, Y.; Ebashi, T.; Ito, S.-i.; Kubota, T.; Kunimori, K.; Tomishige, K. *Chem. Commun.* **2009**, 5308.
(18) Alayoglu, S.; Nilekar, A. U.; Mavrikakis, M.; Eichhorn, B. *Nat. Mater.* **2008**, *7*, 333.
(19) Liu, W.; Flytzani-Stephanopoulos, M. *J. Catal.* **1995**, *153*, 304.
(20) Liu, Y.; Fu, Q.; Stephanopoulos, M. F. *Catal. Today* **2004**, *93*−*95*, 241.
(21) Hornes, A.; Hungira, A. B.; Bera, P.; Lopez Camara, A.; Fernandez-Garcia, M.; Marinez-Arias, A.; Barrio, L.; Estrella, M.; Zhou, G.; Fonseca, J. J.; Hanson, J. C.; Rodiguez, J. A. *J. Am. Chem. Soc.* **2010**, *132*, 34.
(22) Rossignol, C.; Arrii, S.; Morfin, F.; Piccolo, L.; Caps, V.; Rousset, J.-L. *J. Catal.* **2005**, *230*, 476.
(23) Wu, J.; Kubiak, C. P. *J. Am. Chem. Soc.* **1983**, *105*, 7456.
(24) Yamazaki, S.-i.; Ioroi, T.; Yamada, Y.; Yasuda, K.; Kobayashi, T. *Angew. Chem., Int. Ed.* **2006**, *45*, 3120.
(25) Kim, W. B.; Voitl, T.; Rodriguez-Rivera, G. J.; Dumesic, J. A. *Science (Washington, DC)* **2004**, *305*, 1280.
(26) Sherry, A. E.; Wayland, B. B. *J. Am. Chem. Soc.* **1990**, *112*, 1259.
(27) Nelson, A. P.; DiMagno, S. G. *J. Am. Chem. Soc.* **2000**, *122*, 8569.
(28) Kadish, K. M.; Li, J.; Van Caemelbecke, E.; Ou, Z.; Guo, N.; Autret, M.; D'Souza, F.; Tagliatesta, P. *Inorg. Chem.* **1997**, *36*, 6292.
(29) Mu, X. H.; Kadish, K. M. *Inorg. Chem.* **1989**, *28*, 3743.
(30) Shi, C.; Anson, F. C. *Inorg. Chem.* **2001**, *40*, 5829.
(31) Van Baar, J. F.; Van Veen, J. A. R.; De Wit, N. *Electrochim. Acta* **1982**, *27*, 57.
(32) Zhang, X.-X.; Parks, G. F.; Wayland, B. B. *J. Am. Chem. Soc.* **1997**, *119*, 7938.
(33) Fu, X.; Li, S. L.; Wayland, B. B. *Inorg. Chem.* **2006**, *45*, 9884.
(34) Hendriksen, D. E.; Eisenberg, R. *J. Am. Chem. Soc.* **1976**, *98*, 4662.
(35) Sun, H.; Xue, F.; Nelson, A. P.; Redepenning, J.; DiMagno, S. G. *Inorg. Chem.* **2003**, *42*, 4507.
(36) Dolphin, D.; Traylor, T. G.; Xie, L. Y. *Acc. Chem. Res.* **1997**, *30*, 251.
(37) *The Porphyrin Handbook*; Kadish, K. M., Smith, K. M., Guilard, R., Eds.; Academic Press: New York, 1999; Vol. 1.
(38) Woller, E. K.; DiMagno, S. G. *J. Org. Chem.* **1997**, *62*, 1588.
(39) Biffinger, J. C.; Sun, H.; Nelson, A. P.; DiMagno, S. G. *Org. Biomol. Chem.* **2003**, *1*, 733.
(40) Krishnamurthy, M. *Inorg. Chim. Acta* **1977**, *25*, 215.
(41) Ashley, K. R.; Shyu, S.-B.; Leipoldt, J. G. *Inorg. Chem.* **1980**, *19*, 1613.
(42) Fu, X.; Wayland, B. B. *J. Am. Chem. Soc.* **2004**, *126*, 2623.
(43) Fu, X.; Basickes, L.; Wayland, B. B. *Chem. Commun* **2003**, 520.
(44) Grass, V.; Lexa, D.; Momenteau, M.; Saveant, J.-M. *J. Am. Chem. Soc.* **1997**, *119*, 3536.
(45) Grass, V.; Lexa, D.; Saveant, J.-M. *J. Am. Chem. Soc.* **1997**, *119*, 7526.
(46) Collman, J. P.; Boulatov, R. *J. Am. Chem. Soc.* **2000**, *122*, 11812.
(47) Aoyama, Y.; Tanaka, Y.; Fujisawa, T.; Watanabe, T.; Toi, H.; Ogoshi, H. *J. Org. Chem.* **1987**, *52*, 2555.
(48) Lexa, D.; Grass, V.; Saveant, J.-M. *Organometallics* **1998**, *17*, 2673.
(49) Collman, J. P.; Murphy, D. W.; Dolcetti, G. *J. Am. Chem. Soc.* **1973**, *95*, 2687.
(50) Collman, J. P.; Boulatov, R. *Inorg. Chem.* **2001**, *40*, 560.
(51) Sun, H.; Smirnov, V. V.; DiMagno, S. G. *Inorg. Chem.* **2003**, *42*, 6032.
(52) Smirnov, V. V.; Woller, E. K.; DiMagno, S. G. *Inorg. Chem.* **1998**, *37*, 4971.
(53) Cargill, R. W. . In *Solubility Data Series*; International Union for Pure and Applied Chemistry (IUPAC), 1990; Vol. 43, p 19

Supporting Information

Ligand Fluorination to Optimize Preferential Oxidation (PROX) of Carbon Monoxide by Water-Soluble Rhodium Porphyrins

Justin C. Biffinger,[†,‡] ShriHarsha Uppaluri,[†] Haoran Sun,[†,μ] and Stephen G. DiMagno[†,*]

[†]*Department of Chemistry and Nebraska Center for Materials and Nanoscience, University of Nebraska, Lincoln, NE 68588-0304,* [‡]*US Naval Research Laboratory, Chemistry Division, Washington, D.C. 20375, and* [μ] *Department of Chemistry, University of South Dakota, Vermillion, SD 57069*

Experimental Section

Materials & Instruments

Reagents were supplied by Aldrich, Sigma, Fisher, Fluka, or Cambridge Isotope Laboratories and used as received unless otherwise indicated. Research grade gases and gas mixes were purchased from Linweld, Lincoln, NE. NMR spectra were obtained in D_2O using the 300, 400, or 500 MHz spectrometers at the University of Nebraska-Lincoln. Absorption spectra were obtained using a modified (OLIS-14) Cary-14 UV-Vis-NIR or Varian Cary 5000 spectrophotometers equipped with a variable-temperature cell holder and a circulating bath (Laude RC3).Head gas analyses of reactions were performed using a Varian CP-3800 gas chromatograph equipped with HayeSep Q 80/100 mesh and Supelco 13X molecular sieve 45/60 mesh columns and a thermal conductivity detector (TCD). A Fisher Scientific Accumet meter with a combination pH electrode (Ag/AgCl reference, gel-filled) was used for pH determinations. For endpoint titration analyses, all manipulations were conducted using a Schlenk vacuum manifold equipped with a gas-delivery manifold and mercury bubbler. Mass spectra were collected at the University of Nebraska Center for Mass Spectroscopy. Elemental analyses were conducted by QTI, Whitehouse NJ.

Electrochemistry

All electrochemical experiments were performed with a computer controlled EG&G M273A Potentiostat/Galvanostat with M270 electrochemical software. A single compartment cell consisting of a glassy carbon working electrode (either from Cypress (0.018 cm^2) or EG&G (0.031 cm^2)), a homemade Ag/AgCl (sat. aqueous KCl) reference electrode, and a platinum wire counter electrode was used for cyclic voltammetry. The working electrode was polished using an EG&G polishing kit and cleaned by ultrasound prior to each use. Filtered, deionized water (>18 MΩ) was used to prepare the electrolyte

solutions (0.5 M $NaPF_6$, supporting electrolyte, 0.1 M phosphate buffer) and 0.1 M NaOH was used to adjust the solution pH. All electrochemical experiments were performed under nitrogen at room temperature. All potentials are referenced to the Ag/AgCl electrode.

Rotating-disk voltammetry

Reduction of O_2 was performed using a rotating platinum ring-graphite disk electrode. The activated platinum disk electrode was calibrated using quantitative oxygen reduction and hydrogen oxidation measurements in sulfuric acid, as was previously described.[1] The graphite disk was coated with the cationic condensation polymer poly(1,4-diazoniabicyclo[2.2.2]octane-1,4-phenylene methylene dibromide), and **2[Rh(III)]** was immobilized on the disk by ion exchange with the resin. The supporting electrolyte was 0.1M phosphate buffer saturated with oxygen. The platinum ring electrode was held at + 0.8 V to oxidize the H_2O_2 that was generated at the disc electrode. Proton reduction was observed at potentials negative of – 0.6 V versus (Ag/AgCl). Rotating ring/disk voltammograms (S = 10 μA and 2 μA for the disk and the ring currents respectively, scan rate = 2 mV s^{-1}, rotation rate = 100 rpm) show that a substantial fraction (50% for **2[Rh(III)]**) of the dioxygen reduction product is H_2O_2. Representative output is shown in **Figure S12**

Determination of the pK_a of 2[Rh-D]

Samples of **2[Rh(III)]** loaded into 5 mm NMR tubes equipped with a resealable PTFE valves (in deuterium oxide, 20mM phosphate, acetate, or oxalate buffers) were degassed via Schlenk techniques. The evacuated tubes were pressurized with H_2 (1.0 atm) and ^{19}F NMR were collected to determine the acid dissociation constant (298 °K, C_6F_6 int. std.). The observed ^{19}F chemical shift of the β-signal was independent of buffer composition, but strongly dependent on pH. The pH was monitored with a properly calibrated combination pH electrode before and after the NMR experiment. The data were linearized using the Henderson-Hasselbalch equation using the observed NMR shifts and fit with the standard linear regression package in Mathematica 5.0. The limiting chemical shift values used were **2[Rh-D]** = -146 ppm and **2[Rh(I)]** = -151 ppm. The data are plotted in **Figure S2**.

Determination of the UV-Vis profile in Figure S5 for the 2[Rh(III)] catalyzed oxidation of CO by Indigo Carmine

A quartz cuvette modified for Schlenk work was charged with 3 mL of an aqueous solution of **2[Rh(III)]** (0.032 mM) and IC (0.064 mM) buffered at pH 4 (200 mM phosphate buffer). The solution was degassed by freeze-pump-thawing three times directly on the Schlenk line. The cuvette was then pressurized (1 atm) with CO through a mercury bubbler. The cuvette was shaken vigorously for 30 seconds to ensure introduction of CO into solution phase at a uniform concentration, and it was placed in

the temperature controlled (35 °C) cuvette holder. UV-Vis spectra were collected at regular time intervals.

Determination of TOF_{av} of the 2[Rh(III)] catalyzed oxidation of CO by Indigo Carmine

A 5 mm NMR tube equipped with a resealable PTFE valve was charged with 1 mL of an aqueous solution (buffered at pH 4 with a 200 mM phosphate buffer) of **2[Rh(III)]** and IC at the required concentration. The blue solution was degassed by cool (0 °C)-pump-warming (35 °C) ten times directly on a Schlenk line. The tube was then pressurized (1 atm) with pure CO or 50% CO in (N_2 or H_2) through a mercury bubbler. The solution was shaken vigorously for 30 seconds to ensure quick introduction of a uniform concentration of CO into solution and subsequently placed in a 35 °C water bath. The tube was removed from the heating bath every 1.5 min and the solution agitated as for 15 seconds, and was then returned to the heating bath. This procedure was repeated until the blue color of the solution disappeared leaving behind a faintly brown solution characteristic of the color of **2[Rh(I)].**

Scrubbing CO from CO in H_2 gas mixes

A Schlenk flask (total volume 12 mL) was charged with 8.5 mL of an aqueous solution (buffered at pH 4 with a 200 mM phosphate buffer) of **2[Rh(III)]** (0.6 mM) and IC (6.0 mM). A magnetic stir bar was dropped in and the flask was sealed. The solution was degassed by freeze-pump-thawing three times on the Schlenk line. The flask was then pressurized (1 atm) with the required gas mix (10% CO in H_2 or 1% CO in H_2) through a mercury bubbler, transferred to an oil bath maintained at 35 °C, and the solution was set to vigorous stirring. 25 μL aliquots of the head gas were withdrawn using a gas-tight syringe, initially, and from time to time through the progress of the reaction, and analyzed by GC.

Figures and Tables

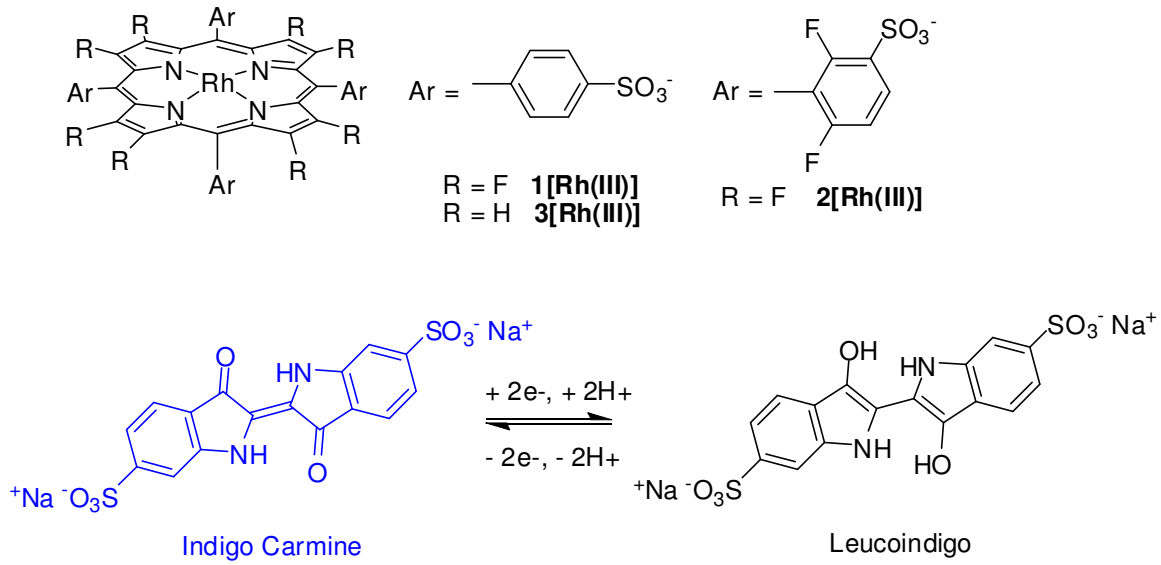

Figure S1. Structures of indigo carmine, leucoindigo, and the porphyrins **1[Rh(III)]** and **2[Rh(III)]** and **3[Rh(III)]**.

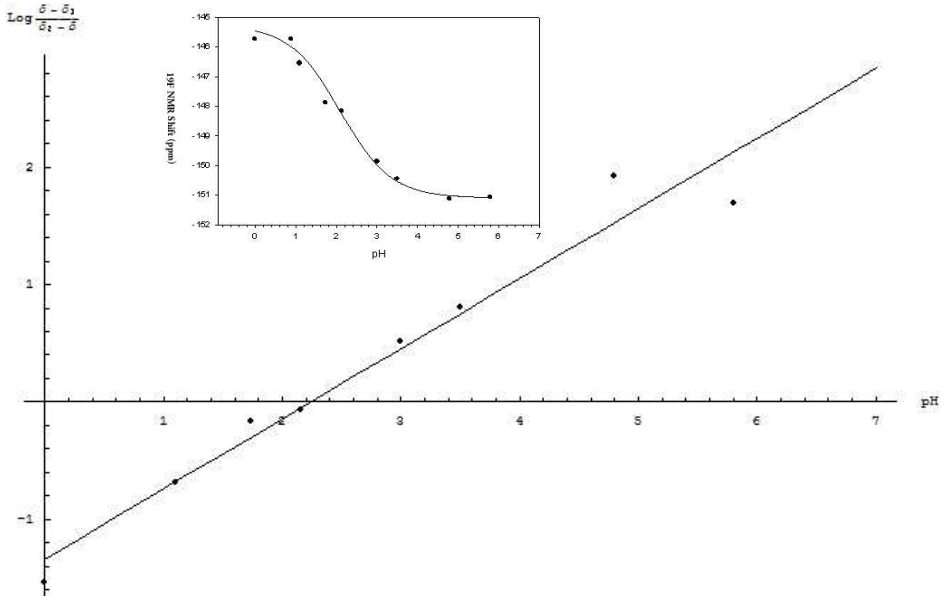

y = -1.33953+0.597393 x (Best Fit Equation)

```
Out[67]= {ParameterTable → 1    Estimate    SE          TStat       PValue
                           -1.33953    0.167774    -7.98414    0.000205717 , RSquared → 0.958202, AdjustedRSquared → 0.951236,
                         x  0.597393   0.050937    11.7281     0.0000231869

                                                  DF    SumOfSq     MeanSq      FRatio      PValue
          EstimatedVariance → 0.0669249, ANOVATable → Model  1     9.20536     9.20536     137.548     0.0000231869}
                                                      Error  6     0.401549    0.0669249
                                                      Total  7     9.60691
```

Figure S2. Determination of pK_a for **2[Rh-D]**

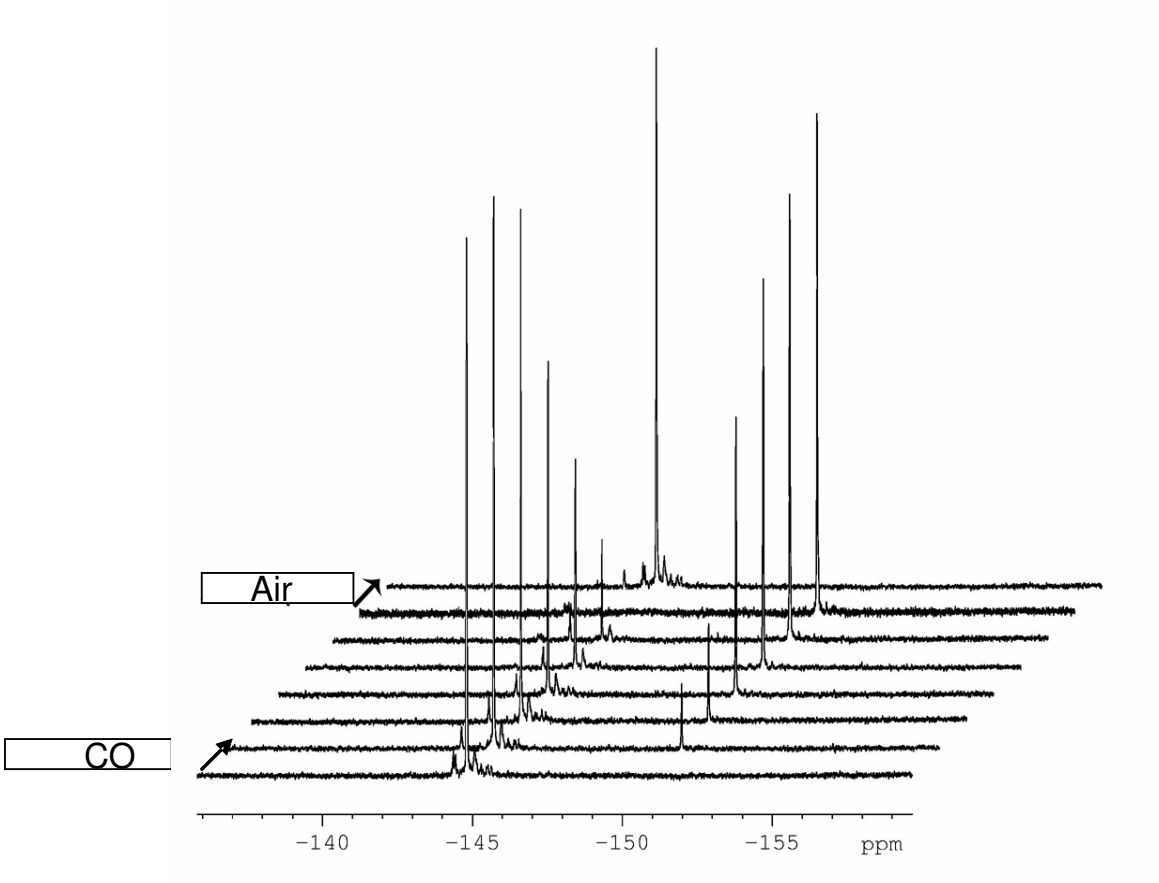

Figure S3. Changes in the ^{19}F NMR during the reaction of **2[Rh(III)]** with CO in D_2O. The peaks at ca. -145 ppm and ca. -151 ppm arise from the β-F on **2[Rh(III)]** and **2[Rh(I)]**$^-$ respectively.

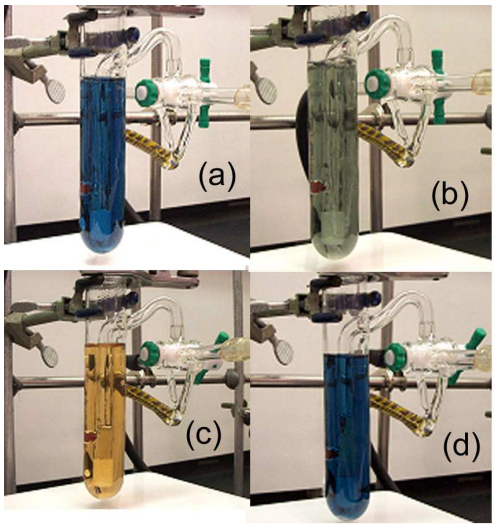

Figure S4. Color changes associated with the **2[Rh(III)]** catalyzed oxidation of CO by indigo carmine at pH 4. a) initial – before CO purge, b) during CO purge, c) end point, d) after introduction of air.

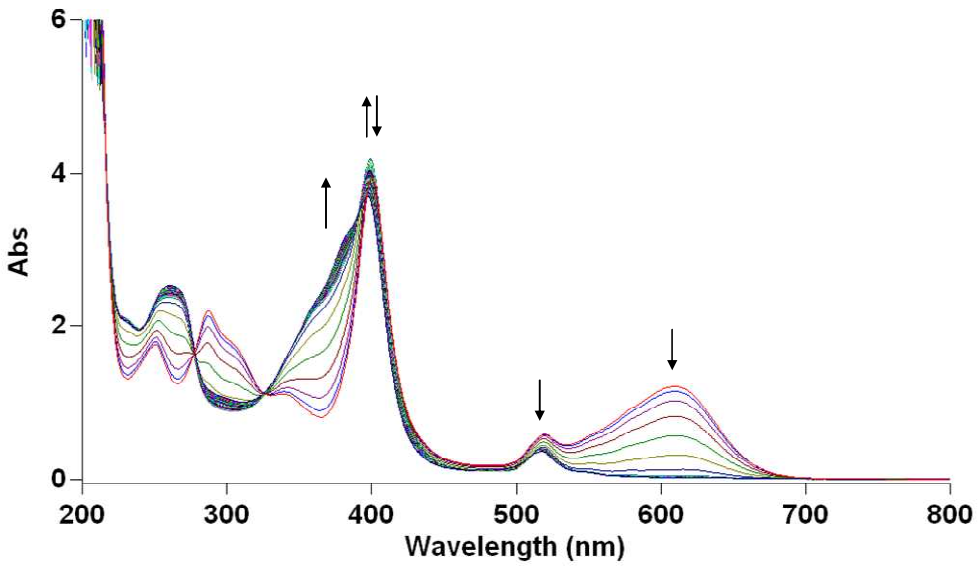

Figure S5. UV-vis spectra of the **2[Rh(III)]** catalyzed oxidation of CO by indigo carmine at pH 4 and 35 °C. Initial concentrations: 0.032 mM **2[Rh(III)]** and 0.064 mM indigo carmine. The progressive decrease in absorbance at 520 nm (which is the λ_{max} for the Q-band of **2[Rh(III)]**) corresponds only to a decrease in absorbance of indigo carmine (See **Figure S6**).

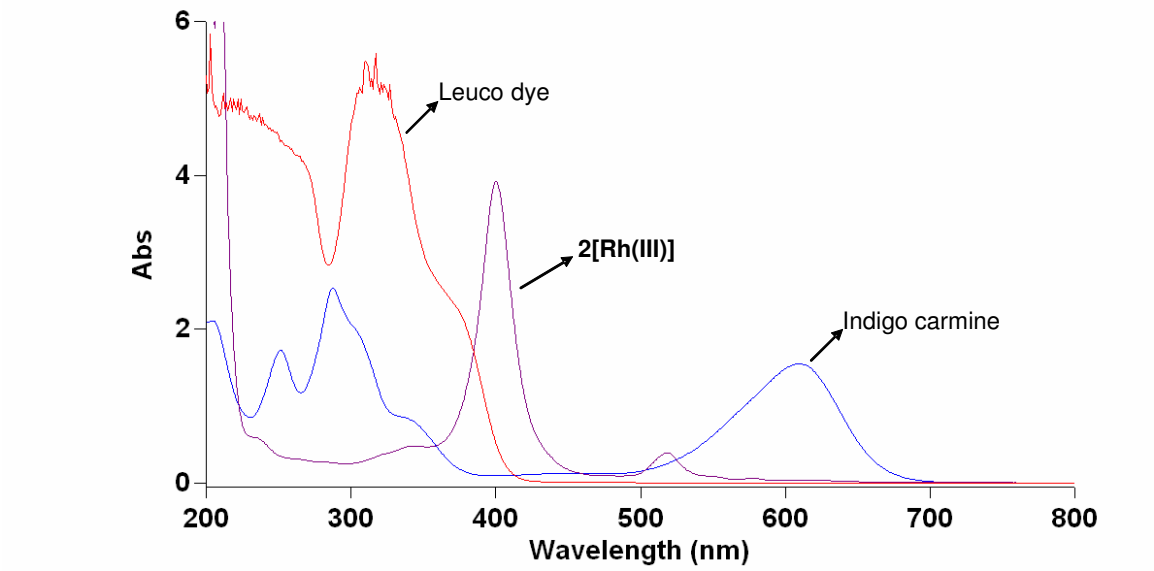

Figure S6. Overlaid UV-vis spectra of 0.064 mM indigo carmine, 0.064 leucoindigo, and 0.032 mM **2[Rh(III)]** in pH 4 aqueous solutions and 35 °C.

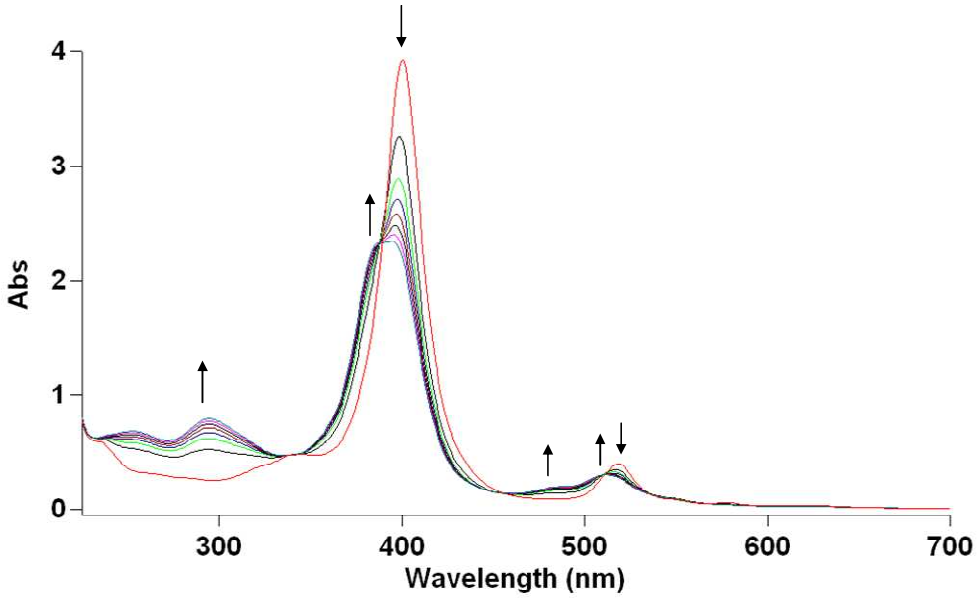

Figure S7. UV-vis profile of the reduction of 0.032 mM **2[Rh(III)]** to **2[Rh(I)]** by 1 atm CO in a pH 4, 200 mM aq. phosphate buffer solution at 35 °C.

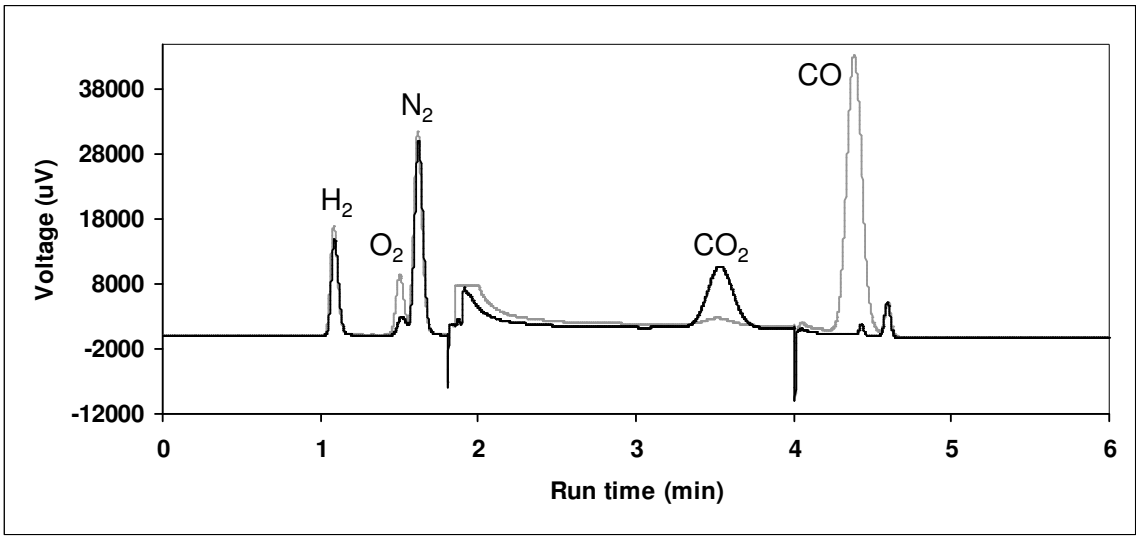

Figure S8. Scrubbing of CO from a 10% CO in H_2 mix (total pressure of 1 atm) by 0.6 mM **2[Rh(III)]** and 6.0 mM indigo carmine in pH = 4 phosphate buffer at 35 °C. The two small peaks at 4.4 and 4.6 minutes were also observed in control (blank) gas injections. The peaks at ~2 min and ~ 4 min are artifacts generated during the valve switching associated with multiple column GC operation (See **Figure S9**).

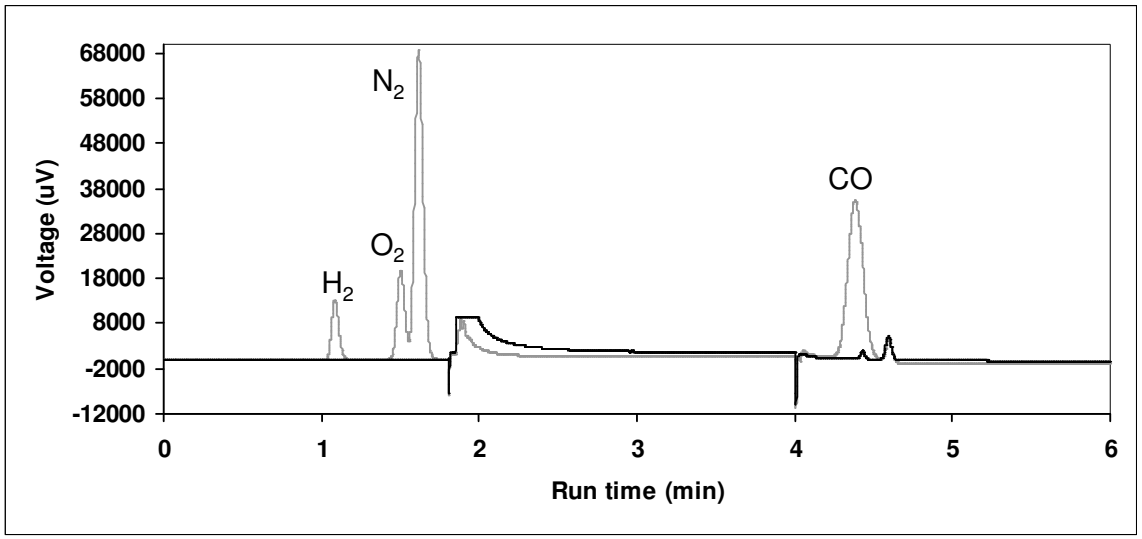

Figure S9. Reference GC traces. Grey trace – 10% CO/H_2 balance. Black trace – helium blank.

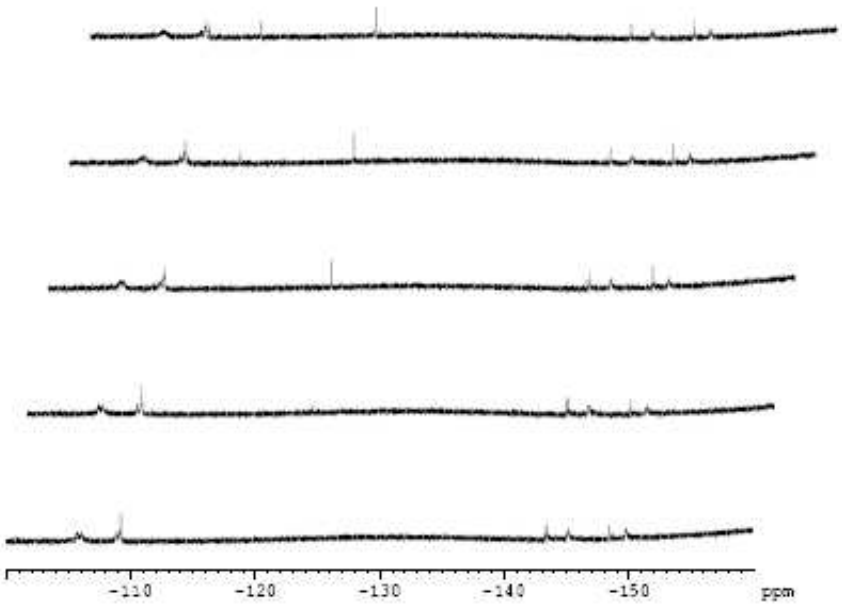

Figure S10. ^{19}F NMR monitoring of a control solution of 1 mM **2[Rh(III)]** + 10 μL of 30% H_2O_2 in 1 mL D_2O at pH 4 over two days. The initial spectrum is at the bottom and the final spectrum is at the top of the figure. The growth of the peak at -121 ppm indicates liberation of fluoride ion from the porphyrin.

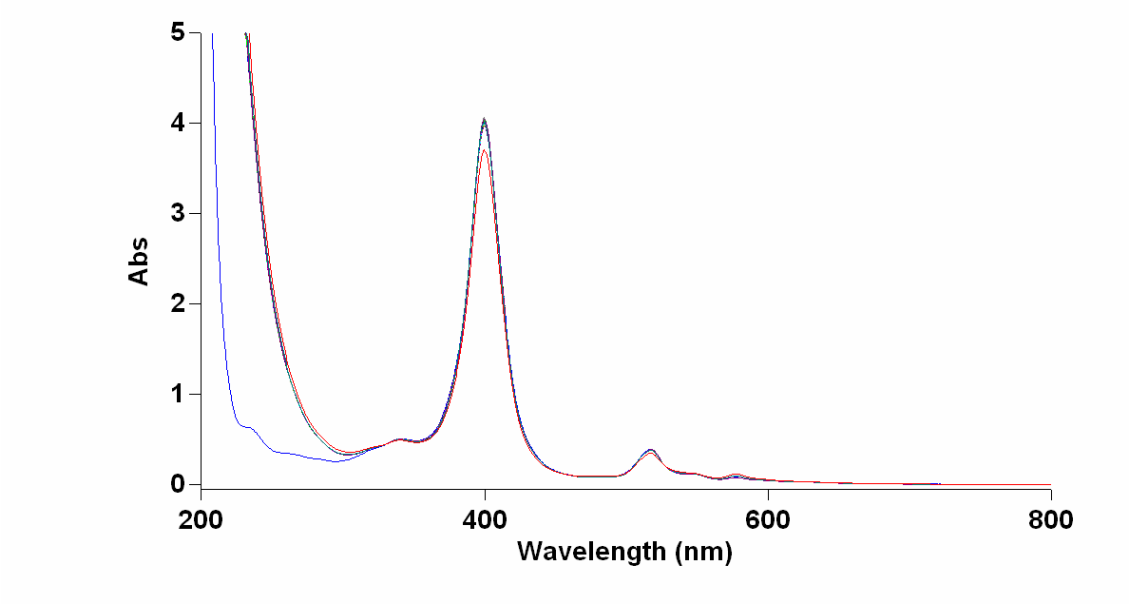

Figure S11. UV-Vis monitoring of a control solution of 0.025 mM **2[Rh(III)]** + 10 µL of 30% H_2O_2 in 1 mL of D_2O at pH 4 over two days. The initial spectrum is in blue, the second spectrum (black) was recorded immediately after the addition of hydrogen peroxide. The final spectrum, recorded after two days, is shown in red.

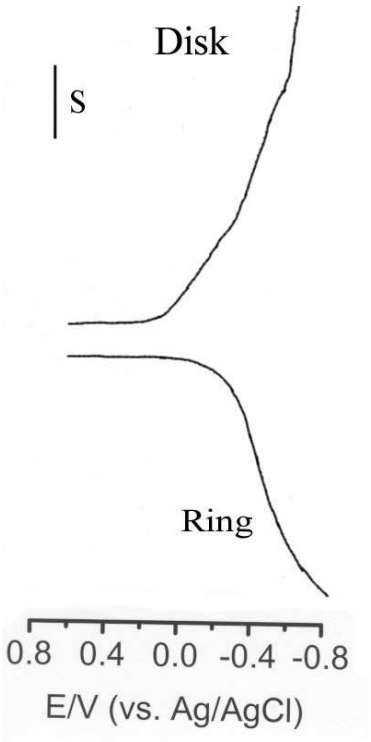

Figure S12. Rotating ring-disk voltammetry of the reduction of O_2 at a graphite disk electrode coated with **2[Rh(III)]**.

Table S1. TOF at pH = 4 for pure CO oxidation at 1 atm pressure, 35 °C (intermediate concentration range of **2[Rh(III)]**)

Run	**2[Rh(III)]** (mM)	IC (mM)	Turnover No. TON	End point (min)	TOF_{av} (TO min^{-1})	Corrected[a] TOF_{av} (TO min^{-1})
1	0.25	1.0	4.0	5.0	0.80	
2	0.25	5.0	20.0	13.5	1.48	1.88
3	0.25	10.0	40.0	24.5	1.63	1.85
4	0.10	1.0	10.0	9.5	1.0	
5	0.10	2.0	20.0	15.0	1.33	1.82
6	0.10	5.0	50.0	31.0	1.61	1.86
7	0.050	0.50	10.0	11.5	0.87	
8	0.050	1.0	20.0	17.5	1.14	1.67
9	0.050	2.0	40.0	27.0	1.48	1.93
10	0.025	0.25	10.0	21.0	0.48	
11	0.025	0.50	20.0	26.0	0.77	2.0

a. The corrected TOF_{av} is obtained by calculating the difference in TON (ΔTON/Δtime) for consecutive table entries run under the same conditions. This approach corrects for an initial induction period that arises from scrubbing of residual dissolved O_2. For example, the corrected TOF_{av} for run 5 was calculated by using the difference in TON and the difference in end points between run 5 and run 4 [(20-10) / (15.0-9.5)].

Table S2. TOF at pH = 4 and 35 °C for 50% CO (in N_2 or H_2) oxidation.

Run	**2[Rh(III)]** (mM)	IC (mM)	Turnover No. TON	End pt (min)	TOF_{av} (TO min^{-1})	Corrected[a] TOF_{av} (TO min^{-1})
1	0.10	1.0	10.0	16.0	0.62	
2	0.10	2.0	20.0	27.0	0.74	0.91
3	0.025	0.25	10.0	46.0	0.22	
4	0.025	0.50	20.0	57.5	0.35	0.87

a. Defined and calculated in the same way as for the data in **Table S1**.

From the above data it can be seen that the TOF_{av} halves when the partial pressure of CO is halved, thereby indicating a 1st order kinetic dependence on CO partial pressure. The TOF_{av} remained the same independent of the identity of the carrier gas (N_2 or H_2) for the 50% CO gas mixture.

(1) Feltham, A. M.; Spiro, M. *Chem. Rev.* **1971**, *71*, 177-93.
(2) Biffinger, J. C.; Sun, H.; Nelson, A. P.; DiMagno, S. G. *Org. Biomol. Chem.* **2003**, *1*, 733-736.
(3) Ashley, K. R.; Shyu, S.-B.; Leipoldt, J. G. *Inorg. Chem.* **1980**, *19*, 1613-16.
(4) Fu, X.; Wayland, B. B. *J. Am. Chem. Soc.* **2004**, *126*, 2623-2631.